Article

Cell
PRESS

UA62784 Is a Cytotoxic Inhibitor of Microtubules, not CENP-E

Sergey Tcherniuk,[1,2] Sébastien Deshayes,[1,2] Vasiliki Sarli,[3] Gilles Divita,[1,2] and Ariane Abrieu[1,2,*]
[1]Université de Montpellier Sud de France, CRBM
[2]CNRS - UMR 5237, 1919 Route de Mende
34293 Montpellier Cedex 05, France
[3]Faculty of Chemistry, Aristotle University of Thessaloniki, University Campus, 54124 Thessaloniki, Greece
*Correspondence: ariane.abrieu@crbm.cnrs.fr
DOI 10.1016/j.chembiol.2011.03.006

SUMMARY

A recent screen for compounds that selectively targeted pancreatic cancer cells isolated UA62784. We found that UA62784 inhibits microtubule polymerization in vitro. UA62784 interacts with tubulin dimers ten times more potently than colchicine, vinblastine, or nocodazole. Competition experiments revealed that UA62784 interacts with tubulin at or near the colchicine-binding site. Nanomolar doses of UA62784 promote the accumulation of mammalian cells in mitosis, due to aberrant mitotic spindles, as shown by immunofluorescence and live cell imaging. Treatment of cancerous cell lines with UA62784 is lethal, following activation of apoptosis signaling. By monitoring mitotic spindle perturbations and apoptosis, we found that the effects of UA62784 and of some known microtubule-depolymerizing drugs are additive. Finally, high content screening of H2B-GFP HeLa cells revealed that low doses of UA62784 and vinblastine potentiate each other to inhibit proliferation.

INTRODUCTION

Antimitotic drugs have long been used for the treatment of cancers, and they usually target microtubules (MTs). Microtubules are polymers composed of α/β-tubulin dimers, organized in hollow cylinders whose dynamic instability is highly regulated. In interphase, microtubules are essential to various processes such as cell shape, vesicle transport, and cell signaling. Upon mitotic entry, the nature and properties of microtubule-associated proteins dramatically switch to promote shorter and more dynamic microtubules that will organize into a bipolar spindle. This apparatus ensures alignment of the chromosomes at the metaphase plate, a prerequisite for accurate chromosomes partitioning in two identical sets (Gadde and Heald, 2004). This step is subjected to a surveillance mechanism called the "spindle assembly checkpoint" which monitors attachment and biorientation of kinetochores, and depends upon several proteins, including the kinesin CENP-E and the kinase BubR1/BUB1B (Mao et al., 2005; Weaver et al., 2003). Once chromo-

somes are segregated, remodeling of the spindle microtubule network results in the formation of the central spindle, a key structure of the cytokinesis machinery.

The wide class of microtubule-targeting drugs is composed of dozens of molecular backbones (Calligaris et al., 2010) interacting with at least four tubulin binding sites: the taxane site, the colchicine site, the vinca alkaloid site, and one or several uncharacterized domain(s) (Smith and Jordan, 2010). Binding to the taxane site stabilizes MTs. Vinca alkaloids and colchicine are generally known as MT depolymerizing agents but it has also been shown that at low, clinically relevant doses, they stabilize MTs by decreasing microtubule dynamics (Jordan and Wilson, 2004; Okouneva et al., 2008). The mode of binding to tubulin differs between the three main types of compounds. Taxanes preferentially bind to polymerized MTs, at the inner surface of the β subunit (Nogales et al., 1998). In contrast, colchicine binds with high affinity to soluble tubulin but can become copolymerized into MTs. Colchicine binding to β-tubulin prevents curved tubulin from adopting a straight structure, due to a steric clash between colchicine and α-tubulin, which inhibits MT assembly (Ravelli et al., 2004). Finally, the vinca alkaloids generally bind with high affinity to one or a few tubulin molecules at the tip of MTs but do not copolymerize into MTs. Indeed, vinblastine prevents self-association of tubulin by interacting at the interface between two heterodimers (Gigant et al., 2005).

Vinca alkaloids such as vinblastine and vincristine are used in clinics since the 1960s, mainly to treat leukemia and lymphomas or certain advanced cancers. Their clinical efficiency in combination therapies motivated the development of semisynthetic vinca analogs, including vindesine, vinorelbine, and vinflunine, which are also efficient anticancer drugs. Taxol/paclitaxel and its semisynthetic analog Docetaxel/Taxotere are also used as chemotherapeutic agents to treat a wide variety of solid tumors. Colchicine is not used for cancer treatment, probably due to high levels of toxicity, but other molecules targeting the colchicine-binding sites are under investigation for cancer treatment (Jordan and Wilson, 2004).

There are several caveats with these treatments, which stimulate active research to keep developing alternatives (Screpanti et al., 2010). Notably, the currently known drugs are still inefficient against several solid tumors, such as kidney, pancreas, or colon carcinomas. During the last decade, novel antimitotics targeting mitosis-specific enzymes such as protein kinases (PLK1, Aurora) (Malumbres and Barbacid, 2007) and molecular motors (Eg5/KIF11, CENP-E) (Wood et al., 2010) have been
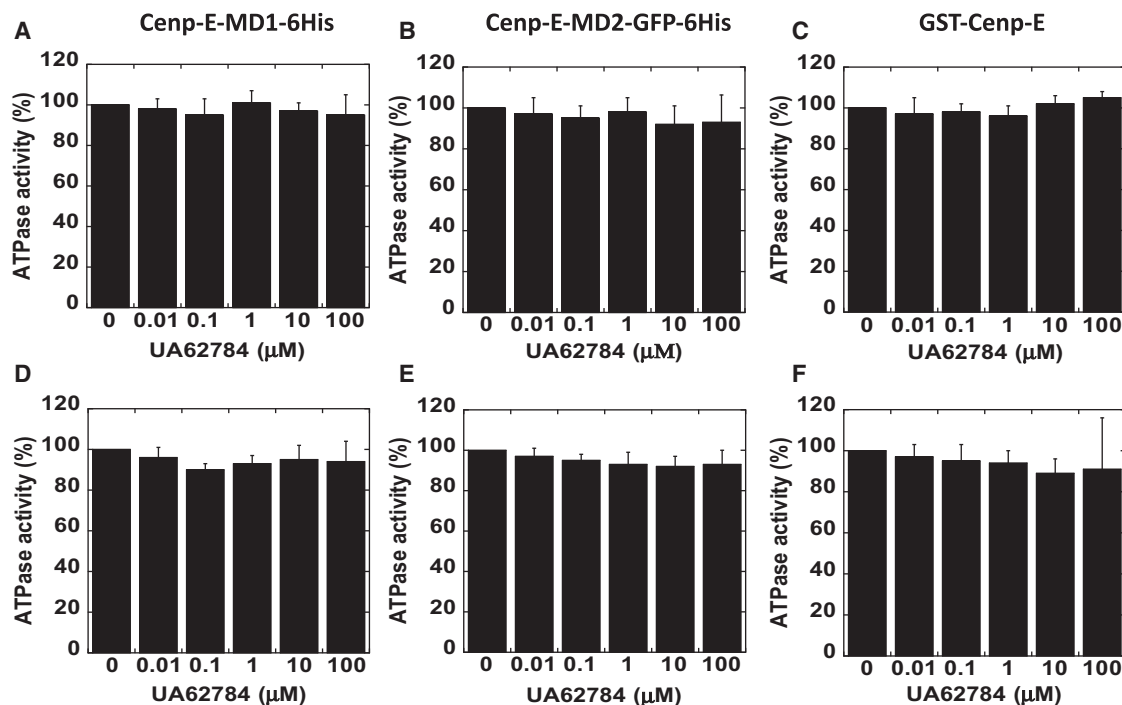
Figure 1. UA62784 Does Not Affect the ATPase Activity of the Kinesin CENP-E

CENP-E ATPase activity was measured by following the release of ADP using the pyruvate kinase/lactate dehydrogenase–linked assay. The tests were performed using three different constructs of CENP-E motor domain (MD): CENP-E-MD1-6His (A and D), CenpE-MD2-GFP-6His (B and E), and GST-CENP-E from Cytoskeleton Inc. (C and F). Basal (A–C) and microtubule-stimulated (D-F) ATPase activities were measured and plotted as the percentage of the activity of the motor in the absence of UA62784. Error bars represent the standard deviation from three independent experiments.

developed. Although some of these drugs are currently in phase II clinical trials, none of them yet appeared to be as potent as microtubule-targeting agents (Dumontet and Jordan, 2010; Huang et al., 2009; Knox et al., 2008; Tang et al., 2008). Finally, the search for novel compounds is also highly motivated by the fact that many cancers eventually develop resistance to these drugs (Kavallaris, 2010).

A recent screen for compounds that selectively targeted pancreas cancer cells isolated UA62784 (Henderson et al., 2009). UA62784 was found to be highly cytotoxic within nanomolar range against human pancreatic cancer cell lines bearing a deletion of the tumor suppressor gene *dpc4* (deleted in pancreas cancer locus 4). Henderson and colleagues attributed the observed UA62784 action to CENP-E inhibition, and UA62784 is being used at such in basic research studies (Maffini et al., 2009). CENP-E is a molecular motor essential for chromosome congression, and for the spindle assembly checkpoint (Abrieu et al., 2000; Weaver et al., 2003). It is also an attractive drug target because its role is strictly restricted to mitosis (Weaver et al., 2007). This prompted us to test UA62784 as an inhibitor of CENP-E, but to our surprise, we found that UA62784 does not inhibit CENP-E ATPase activity in vitro. Strikingly, we found that UA62784 is a potent inhibitor of microtubule polymerization, and we characterized its cytotoxicity, alone or in combination with other known microtubule-targeting agents, using live cell imaging and high content screening of H2B-GFP HeLa cells. We found that UA62784 and vinca alkaloid cytotoxicities are additive or even mildly synergic, which might

provide a strategy to overcome resistance to known MT depolymerizing agents.

RESULTS

UA62784 Binds to Tubulin Dimers at or near the Colchicine-Binding Site and Inhibits Microtubule Formation

We used three constructs of human CENP-E motor domain to measure its ATPase activity, in the presence (Figures 1A–1C) or absence (Figures 1D–1F) of microtubules. We could not detect any inhibition of CENP-E ATPase activity, at any of five doses of UA62784 ranging from 10 nM to 100 μM (Figure 1). Similar results were obtained by measuring release of Pi instead of ADP (data not shown). However, we found that UA62784 prevents microtubule polymerization in MT pull-down experiments (Figure 2B). To better quantify how UA62784 affects tubulin polymerization, we monitored tubulin polymerization by following the increase of the turbidity of the solution at 340 nm. UA62784 inhibits MT polymerization in a dose-dependent manner (Figure 2C), with a half-maximal inhibitory concentration (IC$_{50}$) of 82 ± 20 nM (Figure 2D).

We then investigated the ability of UA62784 to interact with tubulin α/β dimers, using intrinsic tubulin tryptophan fluorescence as a probe (Figure 3A), in comparison with agents known to directly interact with tubulin dimers such as vinblastine (Figure 3B), colchicine (Figure 3C), or nocodazole (Figure 3D). All compounds induced a marked fluorescence quenching upon
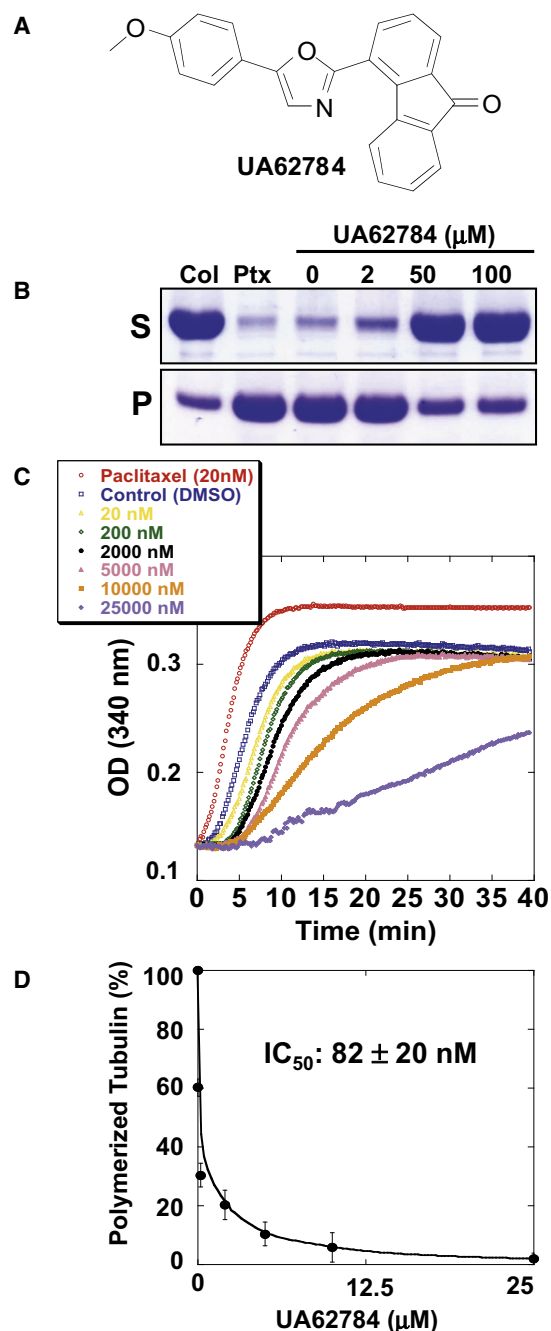
A

UA62784

B

C

D

IC_{50}: 82 ± 20 nM

Figure 2. UA62784 Inhibits Microtubule Polymerization

(A) Chemical structure of UA62784.

(B) Tubulin was polymerized for 5 min at 37°C in the presence of the indicated UA62784 concentrations. Colchicine (Col) (1 μM) and paclitaxel (Ptx) (1 μM) were used as depolymerization and polymerization controls, respectively. After sedimentation, the supernatant (S) and pellet (P) were analyzed by SDS PAGE.

(C) Tubulin was polymerized for 40 min at 37°C in the presence of the indicated concentrations of UA62784 and the absorbance at 340 nm was measured.

(D) The amount of polymerized tubulin in the presence of the indicated doses of UA62784 was measured at 340 nm. Error bars represent the standard deviation from three independent experiments. The concentration required for half-maximal inhibition (IC50) is 82 ± 20 nM.

binding to tubulin α/β dimers, as previously demonstrated for colchicine and vinca alkaloids (Sackett, 1995), while paclitaxel, which preferentially interacts with polymerized tubulin, did not (data not shown). Steady-state fluorescence titrations are biphasic and have been analyzed using a two binding site model: a high affinity site with dissociation constant in the nanomolar range (Kd1) and a low affinity site with dissociation constant in the micromolar range (Kd2). Fitting of UA62784 titration curve (Figure 3A) revealed a high affinity for tubulin with dissociation constants for the first binding mode (Kd1) of 27 ± 13 nM and for the second binding mode of 142 ± 104 μM (Kd2). Considering that Kd2 is more than 5000-fold higher than Kd1, the second binding mode can be negligible for UA62784. Kd1 values for vinblastine (227 ± 45 nM), colchicine (324 ± 36 nM), or nocodazole (259 ± 86 nM) indicated a roughly ten times lower affinity of these drugs over UA62784 for tubulin. In contrast, affinity for the second binding mode is 2- (vinblastin and Colchicine) to 8-fold (Nocodazole) higher than for UA62784, suggesting that this second binding site should be taken into account for this last compound. This was previously described for nocodazole (Xu et al., 2002), and might reflect the presence of a mixture of α/β isotypes in tubulin purified from porc brains (Banerjee and Luduena, 1992).

In order to pinpoint UA62784 binding site, we performed a competition experiment in the presence of [3H]-colchicine. As shown in Figure 3E, the interaction of [3H]-colchicine with tubulin is impaired by addition of increasing doses of UA62784. Addition of 2 to 4 μM of UA62784 displaces more than 60% of the [3H]-colchicine bound to tubulin, which is comparable to the displacement achieved by 10 μM of colchicine. On the contrary, even high doses of vinblastine do not alter the interaction of [3H]-colchicine with tubulin. In conclusion, we found that UA62784 directly interacts with tubulin heterodimers at or near the colchicine-binding site, which affects the net amount of polymerized tubulin in vitro.

UA62784 Arrests Mammalian Cells in Mitosis and Promotes Apoptosis

To determine the effect of UA62784 in cellulo, we exposed unsynchronized HeLa cells to increasing concentrations of drug (ranging from 0.02 to 5 μM). The percentage of cells accumulated in G2/M depended on the UA62784 concentration and exposure time (Figure 4A). As shown in Figure 4A by flow cytometry analysis, the cell cycle profile of HeLa cells after 12 or 24 hr of treatment appears to be modified under 20 nM of UA62784. Similar results were obtained with H358 cells (see Figure S1 available online). Quantification of the flow cytometry plots show that 20 nM of UA62784 for 12 hr promotes the doubling of the G2/M population from $21.5\% \pm 2.8\%$ in untreated cells to $40.1\% \pm 1.1\%$ (Figure 4B). At the same time point, $57.7\% \pm 1.5\%$ of the cells are in G2/M upon treatment with 200 nM of UA62784 (Figure 4B). At later time points under 200 nM of UA62784, the G2/M population culminates at $50.6\% \pm 2\%$ (24 hr) or $44.4\% \pm 1.6\%$ (48 hr), concomitantly with an increase in the sub-G1 population (Figure 4B).

Moreover, mitotic index, scored after staining with mitotic protein monoclonal 2 (MPM2) antibody which recognizes proteins sharing a mitosis-specific phosphorylated epitope, shifted from $3\% \pm 0.7\%$ for untreated cells to $32\% \pm 4\%$ for cells treated
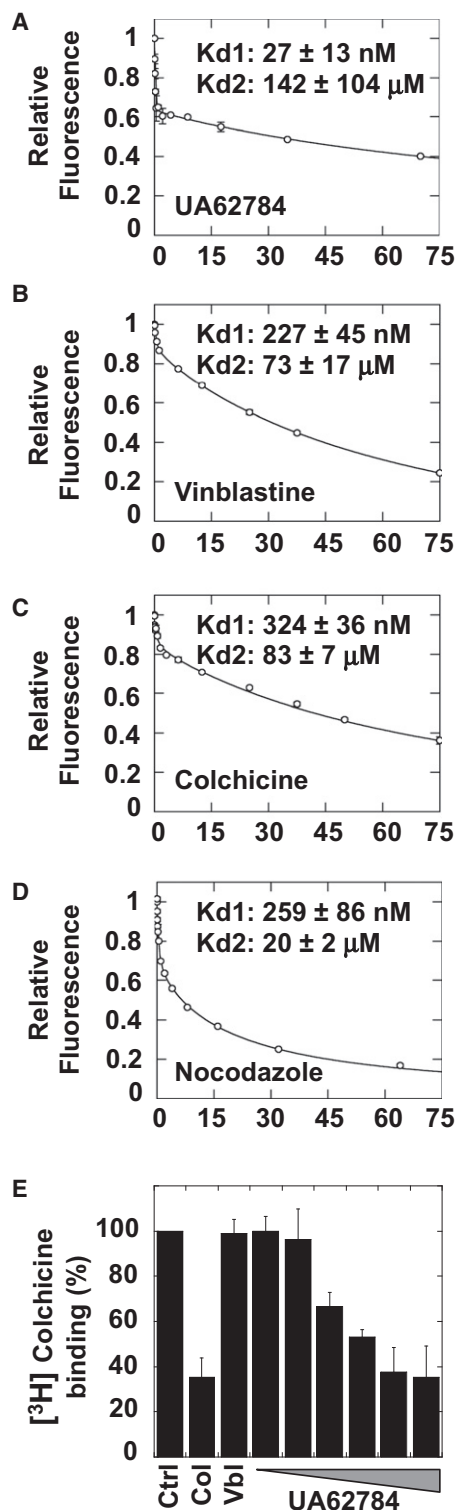
A

Kd1: 27 ± 13 nM
Kd2: 142 ± 104 μM

UA62784

B

Kd1: 227 ± 45 nM
Kd2: 73 ± 17 μM

Vinblastine

C

Kd1: 324 ± 36 nM
Kd2: 83 ± 7 μM

Colchicine

D

Kd1: 259 ± 86 nM
Kd2: 20 ± 2 μM

Nocodazole

E

Figure 3. UA62784 Interacts with Tubulin Heterodimers at or near the Colchicine-Binding Site

Depolymerized tubulin was titrated with 15 nM to 75 μM of UA62784 (A), vinblastine (B), colchicine (C), or nocodazole (D). Normalized fluorescence quenching at 320 nm is fitted with a quadratic equation (see Experimental Procedures). The corresponding dissociation constants are indicated. (E) Tubulin (2 μM) was incubated with [3H]-colchicine (0.13 μM) in the absence of

with 200 nM of UA62784 for 24 hr (Figure 4C). At this dose, western blot analysis showed accumulation of mitotic markers such as Cyclin B, phosphorylated histone H3, and MPM2 (Figure 4D). The persistence of phosphorylated BubR1/BUB1B in this experiment strongly suggests that UA62784-treated HeLa cells are delayed in mitosis due to activation of the spindle assembly checkpoint (Figure 4D).

To examine how UA62784-treated cells eventually escaped from this arrest, we checked for the presence of common effectors of apoptosis by western blot. Activated caspase-3 and -9 and poly-ADP-ribose (PARP-1), were indeed all overexpressed after 24 to 48 hr of UA62784 treatment (Figure 4E). This is consistent with the appearance of increasing amounts of sub-G1 cells upon 24–48 hr of treatment at doses of 20 nM and above (Figure 4B).

To better characterize the effect of UA62784 in mitosis, we stained UA62784-treated cells for tubulin by immunofluorescence and chromosomes with propidium iodide. Microscopy analysis revealed three types of perturbed spindles (Figures 5A and 5B). We define type I spindle as "aberrant but still bipolar," type II as "multipolar," and type III as "depolymerized." The occurrence of these phenotypes were scored for both HeLa and H358 cells treated with UA62784 at concentrations ranging from 20 to 80 nM for 8 hr. More than 70% of mitotic HeLa cells treated with 20 nM of UA62784 display the "type II" phenotype, while at 40 nM, 100% of mitotic cells show no spindle (Figure 5C). H358 cells are slightly more resistant to UA62784, but behave similarly: more than 70% of the cells treated with 40 nM of UA62784 have aberrant but still bipolar spindle, while 100% of cells treated with 80 nM, have a depolymerized spindle (Figure 5D). Time-lapse video microscopy shows that microtubule disruption upon UA62784 treatment occurs within minutes in mitotic (Figure S2) and interphasic (Figure S3) HeLa cells.

Altogether, these results show that UA62784 is a potent inhibitor of microtubules polymerization both in vitro and in cellulo. Cells treated with UA62784 arrest in mitosis and eventually die by apoptosis.

The Effects of UA62784 Are Additive with Vinca Alkaloids, Colchicine, or Nocodazole, but Not Paclitaxel

Since UA62784 is a novel microtubule inhibitor, we decided to compare its effect in mitosis on human cells with the effect of other well-characterized microtubule-targeting agents, such as nocodazole, colchicine, vinblastine and paclitaxel. Meanwhile, we investigated whether the effect of UA62784 in mitosis could be additive with these other drugs. G1/S synchronized HeLa cells were incubated with various drugs either alone or in combination with UA62784 for 12 hr. Figure 6A shows the representative mitotic phenotypes observed by immunofluorescence and Figure 6B display the quantification of these data. In agreement with Figure 5, treatment with 20 nM of UA62784 induces the appearance of perturbed but still bipolar spindles in a majority of cells. However, at this dose of UA62784, further addition of

drug (ctrl), or presence of colchicine (10 μM), vinblastine (20 μM), or increasing concentrations of UA62784 (0.125; 0.25; 0.5; 1; 2 and 4 μM). The amount of [3H]-Colchicine bound to tubulin was determined as described in Experimental Procedures. Error bars represent the standard deviation from three independent experiments.
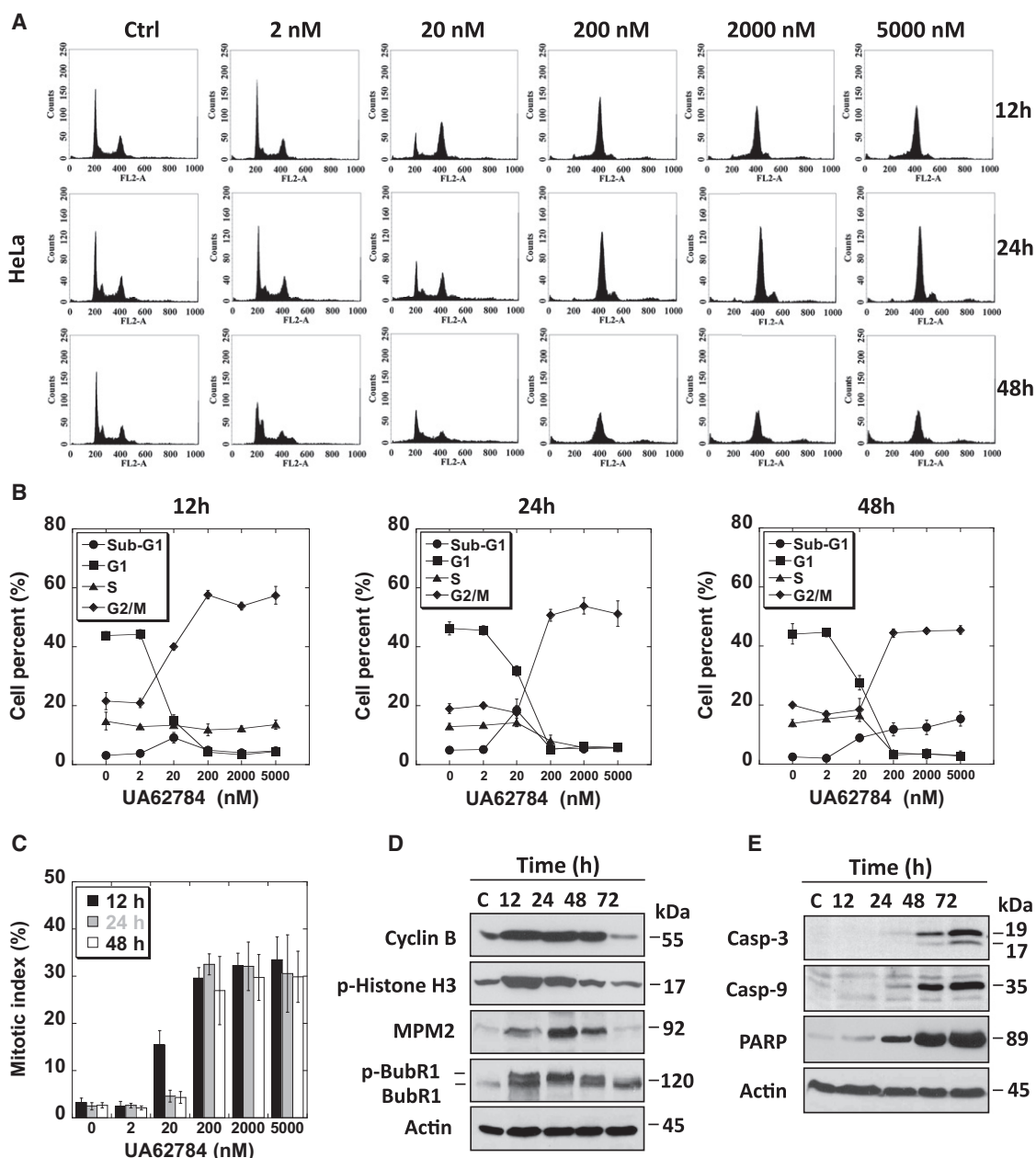
Figure 4. UA62784 Delays HeLa Cells in Mitosis and Promotes Apoptosis

(A) HeLa cells were exposed to the indicated concentrations of UA62784 for 12, 24, and 48 hr and analyzed by flow cytometry.

(B) Quantification of the percentage of cells in Sub-G1, G1, S, and G2/M phases by flow cytometry. (circle) Sub-G1; (square) G1; (triangle) S; (diamond) G2/M.

(C) HeLa cells treated with the indicated concentrations of UA62784 for 12, 24, and 48 hr were fixed with methanol, stained with PI and MPM2-FITC and analyzed by flow cytometry. The average mitotic index of three independent experiments was plotted.

(D) HeLa cells were treated with 200 nM of UA62784 for 12, 24, 48, and 72 hr and the level of the indicated proteins in cell lysates was analyzed by western blot. Actin was used as a loading control.

(E) Activation of apoptotic markers upon UA62784 treatment. HeLa cells were treated with 200 nM of UA62784 for 12, 24, 48, and 72 hr, and the level of activated caspase-3, caspase-9, and PARP were analyzed in cell lysates by western blot.

See also Figure S1.

nocodazole (10 nM) or vinblastine (6 nM) promotes the more severe type III phenotype. Addition of colchicine (1.5 nM) also raises the severity of the mitotic phenotypes induced by UA62784 alone (Figure 6B), while addition of paclitaxel (1.5 nM) does not. Reciprocally, the severity of the mitotic phenotypes induced by nocodazole, colchicine, or vinblastine, but not paclitaxel is worsened by concomitant addition of UA62784. We also followed the fate of the treated cells by flow cytometry in order to quantify the increase in the sub-G1 population, a hallmark of apoptosis (Figure S4). This second readout also shows that the
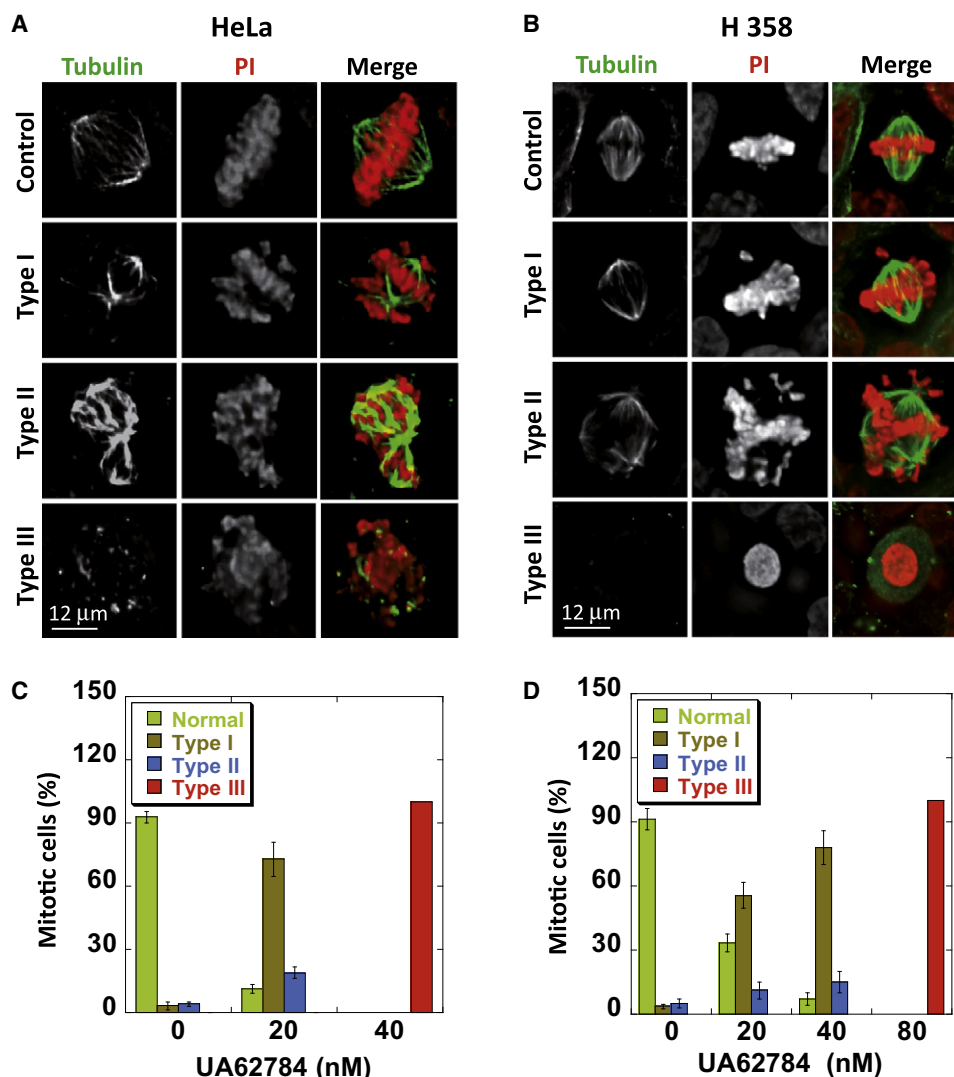
Figure 5. UA62784 Perturbs the Mitotic Spindle

HeLa (A and C) and H358 (B and D) cells were treated with low UA62784 concentrations for 8 hr, fixed, stained with anti-β-tubulin antibody (green) and PI (red), and imaged by fluorescence microscopy (A and B). The ratio of three types of aberrant mitotic phenotypes (see text) was plotted (C and D).

See also Figures S2 and S3. Error bars represent the standard deviation from three independent experiments.

effects of UA62784 and of the three other microtubule-depolymerizing drugs tested are additive, which is not the case with the microtubule-stabilizing agent paclitaxel.

Third, we analyzed how UA62784 alone, or in combination with other drugs, affected cell viability. In this experiment, we included doxorubicin, a DNA intercalant irrelevant to microtubules. To this end, we seeded 96-well plates with equal number of HeLa-H2B-GFP expressing cells to count the number of living cells every 24 hr over 4 days. Each drug was tested alone at six different doses. This allowed us to calculate the dose that inhibits half of the cells growth (IG_{50}). Figure 7A shows that the dose of UA62784 or nocodazole required to kill half of the cells is in the same range (∼30 nM) and similar to vinblastine (∼14 nM), while there is roughly a factor ten of difference, down for paclitaxel (∼1.7 nM) or up for doxorubicin (∼240 nM) in the same conditions. The results from three different fields in the same well

allowed us to draw theoretical additive lines between UA62784 and the other drugs tested (Figure 7B; Table S1), to perform isobolographic analysis of drug combinations. We also combined UA62784 with any one of the other drugs, using three couples of doses, and calculated the corresponding IG_{50}. The results are displayed in Figure 7C and are spotted on the isobolographic graphs in Figure 7B. This shows that cytotoxicity induced by UA62784 and nocodazole or vinblastine is additive, or even mildly synergistic, while ua62784 antagonizes paclitaxel-induced cell death.

DISCUSSION

In the present study, we have carried out an in-depth characterization of the effect of UA62784 as a potent inhibitor of microtubule polymerization both in vitro and in cellulo. Furthermore,
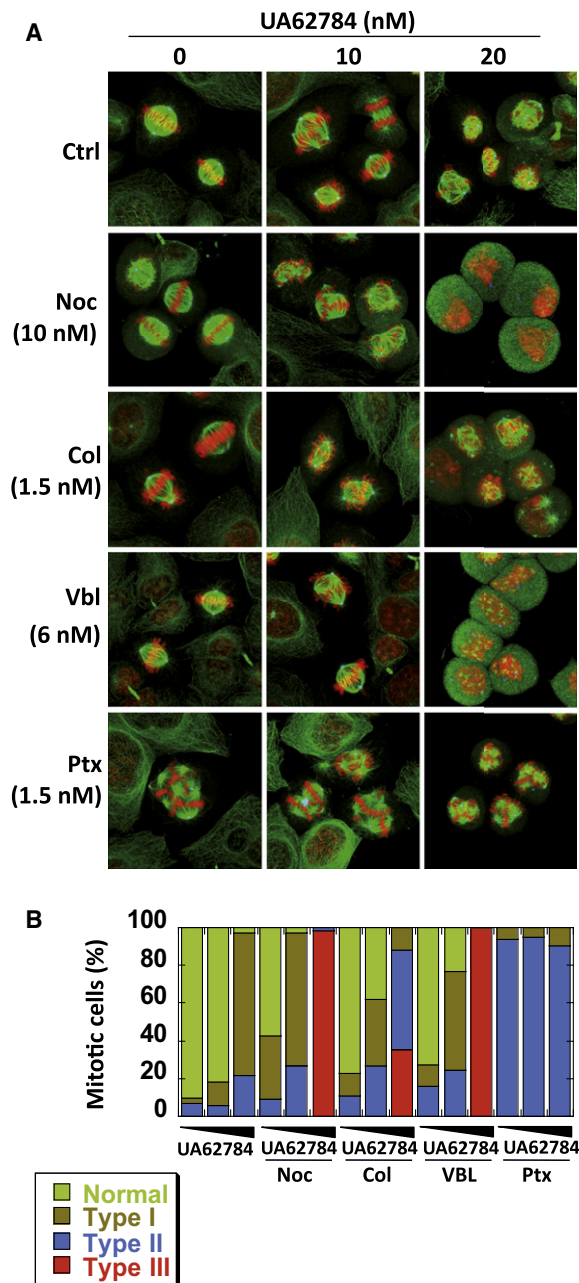
Figure 6. UA62784 and Nocodazole (noc), Colchicine (Col), and Vinblastine (Vbl), but Not Paclitaxel (Ptx) Potentiate Each Other to Perturb the Mitotic Spindle

(A) Representative images of HeLa cells synchronized by Thymidine for 24 hr and released in the presence of the indicated concentration of drugs alone, or in combination for 12 hr. After fixation, the cells were stained with anti-β-tubulin (green), anti-γ-tubulin (blue) antibodies, and PI (red) and imaged by microscopy.

(B) The ratio of normal versus three types of aberrant mitotic phenotypes (see text and Figure 5) from the same experiment is plotted. Three doses of UA62784 (0; 10; 20 nM) are used alone or in combination with nocodazole (10 nM), Colchicine (1.5 nM), vinblastine (6 nM), or paclitaxel (1.5 nM). See also Figure S4.

we have shown that the effects of UA62784 are additive or even synergistic with other microtubule-targeting agents currently used in clinics such as vinca alkaloids. These findings could have positive outcomes for future treatment of cancers. Indeed, UA62784 and one of its derivative, PC-046 are particularly cytotoxic (low nanomolar range) in human pancreatic cancer cell line BxPC3 (Shaw et al., 2009).

UA62784 was initially described as an inhibitor of the mitotic kinesin CENP-E at micromolar doses (Henderson et al., 2009) but in our hands, this is not the case. The defects in spindle bipolarity observed by Henderson and colleagues after UA62784 treatment at nanomolar concentrations already suggested the presence of other cellular targets. Furthermore, β-tubulin staining in Panc-1 cells showed that UA62784 treatment induces microtubule depolymerization. Finally, a subsequent study performed on UA62784 and on a library of 80 analogs, showed that these diaryl oxazole compounds inhibit several protein kinases at micromolar doses, but not kinesins (Shaw et al., 2009). We therefore conclude that the original effects observed upon treatment with low doses of UA62784 were misinterpreted as the result of CENP-E inhibition. Indeed, the phenotype of CENP-E gene knockout (Putkey et al., 2002) is very similar to the one observed in Figure 5B (type I).

Strikingly, we observe a good correlation between the half-maximal concentration of UA62784 required to inhibit tubulin polymerization ($\sim$ 82 nM), the dissociation constant of UA62784 from α/β tubulin ($\sim$ 27 nM), and the half-maximal dose required to inhibit the growth of HeLa cells ($\sim$ 31 nM), which confirmed the implication of the first binding mode of UA62784 to tubulin in the inhibition. This could indicate that UA62784 kills cancer cells mainly by enhancing tubulin depolymerization. However, the multipolar spindles or mono-oriented chromosomes trapped at the pole that we observed after 8 hr of drug treatment suggests that UA62784 also suppresses microtubule dynamics, like vinca alkaloids (Jordan and Kamath, 2007). Furthermore, due to the high intracellular concentration of tubulin, MTs targeting drugs usually accumulate at higher concentrations in cells over that in medium (Jordan and Kamath, 2007). Whether this is also the case for UA62784 remains to be determined.

Structurally, UA62784 incorporates an oxazole core that carries a fluorenone substituent at C-2 (Figure S5). A literature survey shows that oxazole-based compounds (1–3) and fluorenone derivatives (4, 5) bind to microtubules and act as antimitotic agents (Oertel et al., 1992; Stefely et al., 2010; Wang et al., 2002; Wipf et al., 2002). Notably, oxazoles of type 1, 3 exhibit antitubulin and cytotoxic activity by binding to the colchicine site with IC$_{50}$ values in the micromolar range. The compounds binding to the colchicine site inhibit formation of the Cys239 and Cys354 crosslink in β-tubulin and stimulate a GTPase reaction uncoupled from microtubule assembly (Hamel, 1996). A common structural motif in these compounds is the presence of at least one and generally two oxygenated phenyl residues. Guided by the structure of UA62784, we performed competition experiments between UA62784 and [^{3}H]-colchicine, which revealed that UA62784 interacts with tubulin at or near the colchicine-binding site. These data are further supported by our preliminary docking experiments using the molecular modeling program AUTODOCK 4.0 (Morris et al., 1998), which revealed a molecular conformation of UA62784 within the

A | Experimental values of IG_{50} (nM)

Drugs	UA62784 (0 nM)	UA62784 (5 nM)	UA62784 (10 nM)	UA62784 (20 nM)
UA62784	31 ± 1	–	–	–
Nocodazole	35.8 ± 0.8	25.3 ± 1	10.1 ± 0.9	8.8 ± 0.2
Vinblastine	13.9 ± 0.2	10.9 ± 0.2	7.2 ± 0.2	3.7 ± 0.3
Paclitaxel	1.7 ± 0.002	1.7 ± 0.1	1.6 ± 0.1	0.9 ± 0.04
Doxorubicine	240 ± 8	240.2 ± 15	233.8 ± 10	218 ± 11

B

C | Values of combination index (CI), interaction effect (IE) and probability of error (p)

Drugs	UA62784 (5 nM) CI	IE	p	UA62784 (10 nM) CI	IE	p	UA62784 (20 nM) CI	IE	p
Nocodazole	0.86 ± 0.03	SS	p<0.001	0.60 ± 0.02	S	p<0.001	0.89 ± 0.006	SS	p<0.001
Vinblastine	0.95 ± 0.02	NA	p<0.001	0.84 ± 0.01	MS	p<0.001	0.91 ± 0.003	NA	p<0.001
Paclitaxel	1.16 ± 0.05	SA	p<0.01	1.26 ± 0.05	MA	p<0.01	1.18 ± 0.009	SA	p<0.01
Doxorubicine	1.32 ± 0.07	MA	p<0.01	1.61 ± 0.06	A	p<0.01	2.14 ± 0.075	A	p<0.01

S: Synergism, **MS**: Moderate Synergism; **SS**: Slight Synergism; **NA**: Nearly Additive
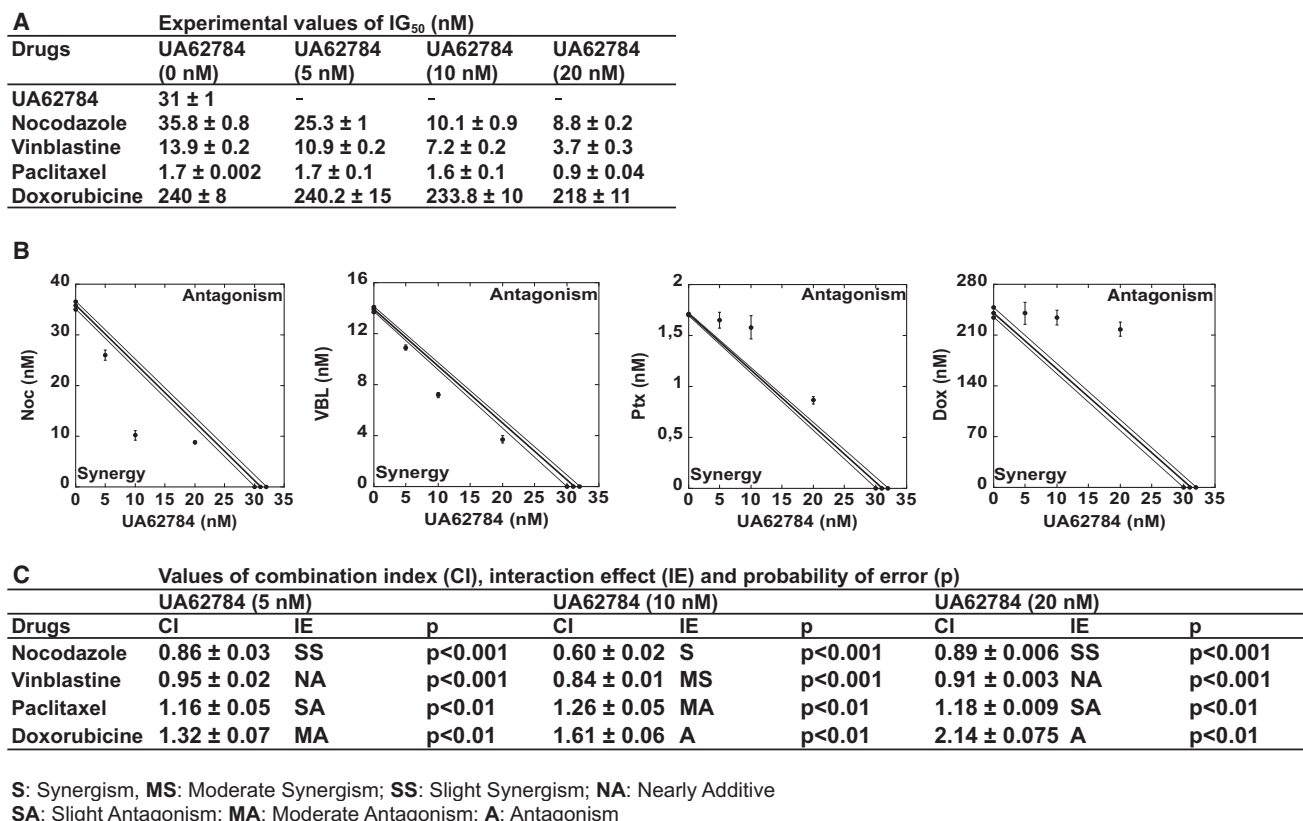**SA**: Slight Antagonism; **MA**: Moderate Antagonism; **A**: Antagonism

Figure 7. UA62784 Synergizes with Vinblastine or Nocodazole, but Antagonizes with Paclitaxel or Doxorubicine to Inhibit the Proliferation of HeLa Cells

(A) Growth inhibition (IG_{50}) of HeLa H2B-GFP cells was quantified by fluorescence using high content cell screening (Cellomics) at 0; 1; 2; 3; and 4 days after treatment with a range of concentrations for the indicated drugs either alone, or in combination with 5 nM; 10 nM or 20 nM of UA62784.

(B) Isobolographic analysis of pharmacodynamic interactions between UA62784 and the indicated drugs. Plotting of the IG_{50} in experiments where UA62784 was added in combination to the other indicated drugs, relative to theoretical additive lines (see Table S1) indicate synergy between UA62784 and nocodazole or vinblastine, and antagonism between UA62784 and paclitaxel or doxorubicine.

(C) Values of the corresponding combination indexes (CI), interaction effect (IE) and probability of error (P-value) determined by t-criterion of Student for paired data.

Error bars represent the standard deviation from three independent experiments.

colchicine-binding site of β-tubulin notably closer to the podophyllotoxin conformation (Ravelli et al., 2004). Furthermore, the docking model revealed a potential H-bond formed with Thr-179 and the carbonyl group of UA62784 (data not shown). According to our results, UA62784 represents a novel antitubulin chemotype and a potent inhibitor of tubulin polymerization. Because of its structural simplicity compared with the well-known vincas or taxanes and their potent cytotoxicity, UA62784 is a very attractive lead compound for further structural modifications and modeling investigations.

In this study, we have provided the first insight into the mechanism of anticancer activity by UA62784. Chemotherapies usually consist of a few hours of treatment on a weekly basis, the tumor therefore experiences only transient exposure to the higher dose of drug. Since UA62784 perturbs the cell cycle over a wide range of concentrations, it is likely to be an efficient drug. The development of clinical drug resistance is a major obstacle to cancer therapies, and metronomic chemotherapy could be one way to overcome this issue (Pasquier et al.,

2010). Therefore, discovery of new chemotherapeutic drugs and new combinations and schedules for cytostatic agents is an important finding for cancer therapeutics. For example, the use of haloperidol in combination with vinblastine reversed the resistance of K562/VBL cells to vinblastine (Kataoka et al., 2001) and the use of imatinib and nilotinib reversed MRP7-mediated paclitaxel resistance (Shen et al., 2009). Having shown that combination of UA62784 with different drugs can lead to additive or even synergistic effects is encouraging in pursuing that route, provided that in vivo analysis will confirm efficacy in xenograft mouse models.

SIGNIFICANCE

Microtubule-targeting agents remain the most efficient antimitotics used in chemotherapies to treat cancer. In this study, we showed that UA62784 directly targets tubulin via the colchicine-binding site, and that it inhibits microtubule polymerization at nanomolar doses in vitro and in vivo.

UA62784 severely damages the mitotic spindle, delays the cell cycle in mitosis and promotes apoptosis. The antiproliferative effect of UA62784 is additive, or even mildly synergistic with vinca alkaloids, which could provide a strategy to lower the doses, and thus to diminish drug-induced resistance in tumor cells.

EXPERIMENTAL PROCEDURES

Antibodies and Drugs

All drugs were purchased from SIGMA. Polyclonal rabbit antibodies: antiphospho histone H3 (Upstate Biotechnology); anti-BubR1 (Santa Cruz Biotechnology); anti-Pan-actin, anticleaved poly ADP ribose polymerase (PARP), anticleaved Caspase-9, anti-caspase-3 are from Cell Signaling. Mouse monoclonal antibodies: anti-MPM-2 (Upstate Biotechnology), anti-β-tubulin (Sigma), anti-cyclin B1 (Santa Cruz Biotechnology). Secondary antibodies: FITC-conjugated donkey anti-mouse and anti-rabbit antibodies are from Jackson ImmunoResearch. Goat anti-rabbit and anti-mouse HRP-conjugated antibodies are from Promega.

Cloning and Purification of CENP-E Constructs

CENP-E-MD1-6His (aa 1-403) and CENP-E-MD2-6His (aa 1-473) were subcloned by PCR into pET28a and pET21a-GFP respectively, using a full-length human CENP-E construct as the template (a gift from Tim Yen, Pennsylvania). The clones were validated by sequencing. For expression, the plasmids were transformed into competent BL21(DE3) *Escherichia coli* host cells. The overnight grown preculture was transferred into 1 l of 2xYT medium (supplemented with appropriate antibiotics) and grown at 37°C until OD$_{600}$ reached 0.6–1.0. Expression was induced with 0.5 mM IPTG at 20°C for 20–24 hr. The bacterial pellets were frozen in liquid nitrogen, and stored at -80°C. All subsequent purification steps were carried out at 4°C. Cells were resuspended in 20 ml lysis buffer (20 mM PIPES [pH 7.3], 200 mM NaCl, 2 mM MgCl$_2$, 1 mM Na-EGTA, 10 mM imidazole, 0.2 mg/ml DNase, 0.5 mg/ml lyzozyme, and 1 mM PMSF), incubated for 30 min, disrupted three times by sonication for 1 min and centrifuged for 30–40 min at 19,000 rpm (Beckmann rotor JA-25.50). The supernatant was loaded onto a 1 ml Ni-charged His-trap FF column (GE Healthcare) previously equilibrated in buffer A (20 mM PIPES [pH 7.3], 200 mM NaCl, 2 mM MgCl$_2$, 1 mM Na-EGTA, 10 mM imidazole). After washing with buffer A (30 column volumes), the column was extensively washed with buffer A containing 20 mM imidazole. The proteins were eluted with 20 column volumes of buffer A containing 250 mM imidazole and collected in fractions of 1 ml. The fractions containing CENP-E were concentrated using Amicon Ultra concentrators (Millipore) to about 8 mg/ml and loaded onto a Superose 12 column equilibrated with buffer B (20 mM PIPES [pH 7.3], 200 mM NaCl, 2 mM MgCl$_2$, 1 mM β-mercaptoethanol). Purified proteins were collected in fractions of 0.5 ml, analyzed by SDS-PAGE, concentrated to 3–6 mg/ml as described above, aliquoted, frozen in liquid nitrogen and stored at -80°C.

ATPase Activities

All enzymatic reactions were performed at room temperature using a 96-well Polarstar photometer at a final volume of 100 μl per well. Steady-state ATPase rates were measured using the pyruvate kinase/lactate dehydrogenase-linked assay in buffer A25A (25 mM potassium ACES [pH 6.9], 2 mM magnesium acetate, 2 mM Na-EGTA, 0.1 mM Na-EDTA, 1 mM β-mercaptoethanol supplemented with 1 mM MgATP; 2 mM PEP; 0.25 mM NADH; 3–10 μg/ml pyruvate kinase; 3 μg/ml lactate dehydrogenase and 8 μM taxol). In the presence of taxol-stabilized microtubules, 50–80 nM of CENP-E proteins were used for the assay. In the absence of microtubules, the basal ATPase activity was measured using 2–4 μM CENP-E. For optimal inhibitor solubility, the assays were done in the presence of up to 5% DMSO. The data were analyzed using Kaleidagraph 3.0 (Synergy Software, Reading, PA) and Microsoft Excel.

Microtubule Polymerization Assays

Porcine tubulin was prepared as described (Espeut et al., 2008). Tubulin polymerization assays were carried out at 37°C in PEM buffer (100 mM PIPES, 1 mM Na-EGTA, and 1 mM MgCl$_2$ [pH 6.9]) by mixing 60 μM of tubulin, 4% DMSO and the indicated concentrations of drugs, in a total volume of 50 μl. For microtubule-pelleting assays, the mixtures were centrifuged at 50,000 × g for 10 min, and the pellet or supernatant fractions were analyzed by SDS-PAGE. For microtubule-turbidity assays, absorbance at 340 nm was measured in 96-well plates with a Polarstar photometer (BMG, Labtech) every 7 sec.

Steady-State Fluorescence Experiments

Fluorescence experiments were performed on a SPEX-PTI spectrofluorometer at 25°C in PEM buffer supplemented with 10 mM CaCl$_2$. Intrinsic tryptophan fluorescence of tubulin heterodimers was excited at 290 nm with a 2 nm slot, and emission spectra were recorded from 300 to 600 nm, with a spectral band-pass of 8 nm. A fixed concentration of tubulin α/β dimers (0.3 μM) was titrated with increasing drug concentrations from 15 nM to 75 μM. All measurements were corrected for the dilution, and data were fitted (Grafit software, Erithacus) with quadratic equations testing for the existence of one or two binding sites (Pelicano et al., 1997). For the four drugs tested, the best fit was obtained with the "two binding sites" equation:

$$F = F_{ini} - (F_1)\left\{ (K_{d1} + L_0 + E_0) - \left[(K_{d1} + L_0 + E_0)^2 - 4\, E_0\, L_0 \right]\, \tfrac{1}{2} \right\} \Big/ (2\, E_0)$$
$$- (F_2)\{ L_0/(K_{d2} + L_0)\}.$$

F_{ini} is the fluorescence intensity at the start of the titration, F_1 and F_2 are the fluorescence-quenching values induced by the first and the second binding respectively, E_0 is the total concentration of protein, L_0 the total concentration of ligand, and K_{d1} and K_{d2} the dissociation constant for the first and the second binding sites of the drug onto tubulin.

[³H]-Colchicine Tubulin-Binding Assay

Colchicine tubulin-binding assays were done using the centrifugal gel filtration method (Koizumi et al., 2004) with minor modifications. Twelve microliter aliquots of 2 μM purified tubulin in PEM buffer supplemented with 10 mM CaCl$_2$ were incubated with 0.13 μM of [³H]-colchicine (1 mCi/ml; specific activity, 75.5 Ci/mmol; Perkin-Elmer, Melbourne, Australia) in the absence or presence of various drugs for 20 min at room temperature. After the incubation, 10 μl of each sample was loaded onto a 75 μl spin column Zeba Micro Desalt Spin Columns (PierceBiotechnology, Inc.) and centrifuged at 1000 × g for 2 min to obtain the tubulin fraction. After the addition of the scintillation fluid, the radioactivity of [³H]-colchicine-bound tubulin was measured using a LS6500 scintillation counter (Beckman Coulter).

Cell Culture and Flow Cytometry

HeLa and HeLa-H2B-GFP cells were grown in DMEM medium (Invitrogen) and H358 cells were cultivated in RPMI 1640 medium (Invitrogen). Cell cultures were supplemented with 2 mM L-glutamine, 1% penicilin/streptomycin and 10% FBS. All cell lines were maintained in a humid incubator at 37°C in 5% CO$_2$. Cells at 60%–70% of confluence were treated with UA62784 for 12, 24, and 48 hr and subsequently collected by pooling together the nonattached and attached cells. After washing in PBS, cells were fixed with methanol for 20 min at -20°C. To estimate the percent of cells that entered mitosis, cells were incubated for 1 hr at 37°C with anti-MPM2 antibody (1:500). After two washes, the cells were stained with FITC-conjugated anti-mouse antibody (1:250). The suspension of stained cells was analyzed by flow cytometry (Becton Dickinson), using CellQuest software. For each sample 10,000 events were collected and aggregated cells were gated out.

Western Blot

HeLa cells were harvested, washed with PBS and subsequently lysed in buffer (50 mM Tris [pH 7.4], containing 250 mM NaCl, 0.1% NP-40, 0.1 mM PMSF, aprotinine at 10 mg/ml, leupeptine at 10 mg/ml, and 100 mM NaF) for 30 min on ice. Then, the cell lysate was centrifuged for 10 min at 13 000 rpm and the concentration of soluble proteins in supernatant was measured by the Bradford method. Equal amount of proteins (30 mg) were resolved by SDS/PAGE, electro-transferred onto nitrocellulose membrane and treated overnight with the appropriate primary antibody diluted 1:1000. Then the membrane were quickly washed and incubated for 1 hr at room temperature with the secondary HRP-conjugated anti-rabbit or anti-mouse antibody. Finally, the membranes were revealed with ECL (Pierce).

Immunofluorescence Microscopy and Live Cell Imaging

For immunofluorescence, cells were grown on poly-D-lysine–coated cover-slips placed in 60 cm² Petri dishes at least 24–36 hr before drug addition. When cells reached 50%–70% confluence the medium was replaced with a fresh one supplemented with UA62784. After exposure to UA62784, cells were fixed in 2% paraformaldehyde in PBS for 20 min at 37°C and treated with anti-β-tubulin antibody (1:400) and anti-γ-tubulin (1:200) for 1 hr at 37°C. Cells were washed three times in PBS for 10 min at room temperature, and subsequently incubated with a FITC-conjugated donkey anti-mouse or Alexa 633 conjugated anti-rabbit antibodies (1:1000) for 30 min at 37°C. After three PBS washes at room temperature, cells were counterstained with PI at 0.5 mg/ml. Finally, the coverslips were washed in PBS three times for 5 min, and mounted on microscopic slides with Mowiol. Images were captured with a Zeiss AxioimagerZ1 motorized microscope, restored by the deconvolution program Huygens Remote Manager (HMR) and analyzed using the Metamorph software or by LSM-510 META Zeiss confocal micro-scope and analyzed using the ImageJ software. For time-lapse video micro-scopy, we used nonsynchronized HeLa cells stably expressing Histone-H2B fused to GFP or HeLa cells stably expressing tubulin fused to GFP. Cells were filmed with a Zeiss Axiovert 200M inverted microscope or Spining disc Perkin Elmer microscope equipped with an incubation chamber at 37°C in 5% CO_2 and controlled by Metamorph 7.1 software (Molecular Devices, Sunnyvale, CA). Differential interference contrast (DIC) and GFP fluorescence images were taken every 10 min for 72 hr to analyze the proliferation dynamic, or every 2–5 min to visualize the drug effect on interphase and metaphase microtubules.

High-Content Cell Screening

HeLa-H2B-GFP were grown on 96-well plates and imaged every 24 hr during 4 days using a Cellomics Arrayscan VTI Live. The amount of live cells in three different fields was calculated for each well. The rate of cell proliferation was estimated as the percentage of live cells compared to control. The proliferation assay was performed in duplicate in three independent experiments. Doses of single drugs used: UA62784 (0; 10; 20; 40; 80; 160 nM), nocodazole (0; 15; 30; 60; 120; 240 nM), vinblastine (0; 1; 2; 4; 8; 16 nM), paclitaxel (0; 0.5; 1; 2; 4; 8 nM), and doxorubicin (0; 125; 250; 500; 1000; 2000 nM). The statistical significance of the difference between the control and treated groups was determined by t-criterion of Student. P values ≤ 0.01 were considered to be statistically significant.

Drug Combinations Analysis

Isobolograms and combination indexes (CI) were determined from the high content screening data after 96 hr. The concentration of compound that caused a 50% growth inhibition (IG₅₀) was determined for UA62784, nocoda-zole, vinblastine, paclitaxel, and doxorubicin. The isobolograms were gener-ated by dually combining the tested drugs to 5, 10, or 20 nM of UA62784 under the following ratio: 5:1, 2:1 and 1:2, respectively. The CI for UA62784 with the drugs acting via a similar mechanism (mutually exclusive) such as nocodazole, vinblastine and paclitaxel was calculated according to the following equation:

$$CI = (D)_1/(Dx)_1 + (D)_2/(Dx)_2,$$

while the CI for UA62784 with doxorubicine, a drug acting via a totally indepen-dent mechanism (mutually nonexclusive) was calculated with the following equation:

$$CI = (D)_1/(Dx)_1 + (D)_2/(Dx)_2 + (D)_1(D)_2/(Dx)_1(Dx)_2,$$

where $(D)_1$ and $(D)_2$ are the IG₅₀ with the combination of drugs 1 and 2, and $(Dx)_1$ and $(Dx)_2$ are the IG₅₀ of drugs 1 and 2 as single compounds. CI value = 1 indicates an additive effect, CI < 1 suggests synergism and CI > 1 suggests antagonism. Degrees of synergism or antagonism were determined using the CI ranges previously described (Chou, 2006).

SUPPLEMENTAL INFORMATION

Supplemental Information includes five figures and one table and can be found with this article online at doi:10.1016/j.chembiol.2011.03.006.

REFERENCES

Abrieu, A., Kahana, J.A., Wood, K.W., and Cleveland, D.W. (2000). CENP-E as an essential component of the mitotic checkpoint in vitro. Cell 102, 817–826.

Banerjee, A., and Luduena, R.F. (1992). Kinetics of colchicine binding to puri-fied beta-tubulin isotypes from bovine brain. J. Biol. Chem. 267, 13335–13339.

Calligaris, D., Verdier-Pinard, P., Devred, F., Villard, C., Braguer, D., and Lafitte, D. (2010). Microtubule targeting agents: from biophysics to proteo-mics. Cell. Mol. Life Sci. 67, 1089–1104.

Chou, T.C. (2006). Theoretical basis, experimental design, and computerized simulation of synergism and antagonism in drug combination studies. Pharmacol. Rev. 58, 621–681.

Dumontet, C., and Jordan, M.A. (2010). Microtubule-binding agents: a dynamic field of cancer therapeutics. Nat. Rev. Drug Discov. 9, 790–803.

Espeut, J., Gaussen, A., Bieling, P., Morin, V., Prieto, S., Fesquet, D., Surrey, T., and Abrieu, A. (2008). Phosphorylation relieves autoinhibition of the kineto-chore motor Cenp-E. Mol. Cell 29, 637–643.

Gadde, S., and Heald, R. (2004). Mechanisms and molecules of the mitotic spindle. Curr. Biol. 14, R797–R805.

Gigant, B., Wang, C., Ravelli, R.B., Roussi, F., Steinmetz, M.O., Curmi, P.A., Sobel, A., and Knossow, M. (2005). Structural basis for the regulation of tubulin by vinblastine. Nature 435, 519–522.

Hamel, E. (1996). Antimitotic natural products and their interactions with tubulin. Med. Res. Rev. 16, 207–231.

Henderson, M.C., Shaw, Y.J., Wang, H., Han, H., Hurley, L.H., Flynn, G., Dorr, R.T., and Von Hoff, D.D. (2009). UA62784, a novel inhibitor of centromere protein E kinesin-like protein. Mol. Cancer Ther. 8, 36–44.

Huang, H.C., Shi, J., Orth, J.D., and Mitchison, T.J. (2009). Evidence that mitotic exit is a better cancer therapeutic target than spindle assembly. Cancer Cell 16, 347–358.

Jordan, M.A., and Wilson, L. (2004). Microtubules as a target for anticancer drugs. Nature Rev. 4, 253–265.

Jordan, M.A., and Kamath, K. (2007). How do microtubule-targeted drugs work? An overview. Curr. Cancer Drug Targets 7, 730–742.

Kataoka, Y., Ishikawa, M., Miura, M., Takeshita, M., Fujita, R., Furusawa, S., Takayanagi, M., Takayanagi, Y., and Sasaki, K. (2001). Reversal of vinblastine resistance in human leukemic cells by haloperidol and dihydrohaloperidol. Biol. Pharm. Bull. 24, 612–617.

Kavallaris, M. (2010). Microtubules and resistance to tubulin-binding agents. Nature Rev. 10, 194–204.

Knox, J.J., Gill, S., Synold, T.W., Biagi, J.J., Major, P., Feld, R., Cripps, C., Wainman, N., Eisenhauer, E., and Seymour, L. (2008). A phase II and pharma-cokinetic study of SB-715992, in patients with metastatic hepatocellular carci-noma: a study of the National Cancer Institute of Canada Clinical Trials Group (NCIC CTG IND.168). Invest. New Drugs 26, 265–272.

Koizumi, Y., Arai, M., Tomoda, H., and Omura, S. (2004). Oxaline, a fungal alkaloid, arrests the cell cycle in M phase by inhibition of tubulin polymerization. Biochim. Biophys. Acta *1693*, 47–55.

Maffini, S., Maia, A.R., Manning, A.L., Maliga, Z., Pereira, A.L., Junqueira, M., Shevchenko, A., Hyman, A., Yates, J.R., 3rd, Galjart, N., et al. (2009). Motor-independent targeting of CLASPs to kinetochores by CENP-E promotes microtubule turnover and poleward flux. Curr. Biol. *19*, 1566–1572.

Malumbres, M., and Barbacid, M. (2007). Cell cycle kinases in cancer. Curr. Opin. Genet. Dev. *17*, 60–65.

Mao, Y., Desai, A., and Cleveland, D.W. (2005). Microtubule capture by CENP-E silences BubR1-dependent mitotic checkpoint signaling. J. Cell Biol. *170*, 873–880.

Morris, G.M., Goodsell, D.S., Halliday, R.S., Huey, R., Hart, W.E., Belew, R.K., and Olson, A. (1998). Automated docking using a Lamarckian genetic algorithm and an empirical binding free energy function. J. Comput. Chem. *19*, 1639–1662.

Nogales, E., Wolf, S.G., and Downing, K.H. (1998). Structure of the alpha beta tubulin dimer by electron crystallography. Nature *391*, 199–203.

Oertel, B., Vater, W., Wiederhold, E.M., Schulze, W., Baumgart, J., Bohm, K.J., Jelke, E., Tint, I.S., Viklicky, V., and Unger, E. (1992). Fluorenone-azomethines, a novel class of microtubule inhibitors that specifically affect cell proliferation. Acta Histochem. *92*, 74–86.

Okouneva, T., Azarenko, O., Wilson, L., Littlefield, B.A., and Jordan, M.A. (2008). Inhibition of centromere dynamics by eribulin (E7389) during mitotic metaphase. Mol. Cancer Ther. *7*, 2003–2011.

Pasquier, E., Kavallaris, M., and Andre, N. (2010). Metronomic chemotherapy: new rationale for new directions. Nat. Rev. Clin. Oncol. *7*, 455–465.

Pelicano, H., Maury, G., Elalaoui, A., Shafiee, M., Imbach, J.L., Goody, R.S., and Divita, G. (1997). Study of the substrate-binding properties of bovine liver adenosine kinase and inhibition by fluorescent nucleoside analogues. Eur. J. Biochem. *248*, 930–937.

Putkey, F.R., Cramer, T., Morphew, M.K., Silk, A.D., Johnson, R.S., McIntosh, J.R., and Cleveland, D.W. (2002). Unstable kinetochore-microtubule capture and chromosomal instability following deletion of CENP-E. Dev. Cell *3*, 351–365.

Ravelli, R.B., Gigant, B., Curmi, P.A., Jourdain, I., Lachkar, S., Sobel, A., and Knossow, M. (2004). Insight into tubulin regulation from a complex with colchicine and a stathmin-like domain. Nature *428*, 198–202.

Sackett, D.L. (1995). Vinca site agents induce structural changes in tubulin different from and antagonistic to changes induced by colchicine site agents. Biochemistry *34*, 7010–7019.

Screpanti, E., Santaguida, S., Nguyen, T., Silvestri, R., Gussio, R., Musacchio, A., Hamel, E., and De Wulf, P. (2010). A screen for kinetochore-microtubule interaction inhibitors identifies novel antitubulin compounds. PLoS ONE *5*, e11603.

Shaw, A.Y., Henderson, M.C., Flynn, G., Samulitis, B., Han, H., Stratton, S.P., Chow, H.H., Hurley, L.H., and Dorr, R.T. (2009). Characterization of novel diaryl oxazole-based compounds as potential agents to treat pancreatic cancer. J. Pharmacol. Exp. Ther. *331*, 636–647.

Shen, T., Kuang, Y.H., Ashby, C.R., Lei, Y., Chen, A., Zhou, Y., Chen, X., Tiwari, A.K., Hopper-Borge, E., Ouyang, J., et al. (2009). Imatinib and nilotinib reverse multidrug resistance in cancer cells by inhibiting the efflux activity of the MRP7 (ABCC10). PLoS ONE *4*, e7520.

Smith, J.A., and Jordan, M.A. (2010). Determination of drug binding to microtubules in vitro. Methods Cell Biol. *95*, 289–299.

Stefely, J.A., Palchaudhuri, R., Miller, P.A., Peterson, R.J., Moraski, G.C., Hergenrother, P.J., and Miller, M.J. (2010). N-((1-benzyl-1H-1,2,3-triazol-4-yl)methyl)arylamide as a new scaffold that provides rapid access to anti-microtubule agents: synthesis and evaluation of antiproliferative activity against select cancer cell lines. J. Med. Chem. *53*, 3389–3395.

Tang, P.A., Siu, L.L., Chen, E.X., Hotte, S.J., Chia, S., Schwarz, J.K., Pond, G.R., Johnson, C., Colevas, A.D., Synold, T.W., et al. (2008). Phase II study of ispinesib in recurrent or metastatic squamous cell carcinoma of the head and neck. Invest. New Drugs *26*, 257–264.

Wang, L., Woods, K.W., Li, Q., Barr, K.J., McCroskey, R.W., Hannick, S.M., Gherke, L., Credo, R.B., Hui, Y.H., Marsh, K., et al. (2002). Potent, orally active heterocycle-based combretastatin A-4 analogues: synthesis, structure-activity relationship, pharmacokinetics, and in vivo antitumor activity evaluation. J. Med. Chem. *45*, 1697–1711.

Weaver, B.A., Bonday, Z.Q., Putkey, F.R., Kops, G.J., Silk, A.D., and Cleveland, D.W. (2003). Centromere-associated protein-E is essential for the mammalian mitotic checkpoint to prevent aneuploidy due to single chromosome loss. J. Cell Biol. *162*, 551–563.

Weaver, B.A., Silk, A.D., Montagna, C., Verdier-Pinard, P., and Cleveland, D.W. (2007). Aneuploidy acts both oncogenically and as a tumor suppressor. Cancer Cell *11*, 25–36.

Wipf, P., Reeves, J.T., Balachandran, R., and Day, B.W. (2002). Synthesis and biological evaluation of structurally highly modified analogues of the antimitotic natural product curacin A. J. Med. Chem. *45*, 1901–1917.

Wood, K.W., Lad, L., Luo, L., Qian, X., Knight, S.D., Nevins, N., Brejc, K., Sutton, D., Gilmartin, A.G., Chua, P.R., et al. (2010). Antitumor activity of an allosteric inhibitor of centromere-associated protein-E. Proc. Natl. Acad. Sci. USA *107*, 5839–5844.

Xu, K., Schwarz, P.M., and Luduena, R.F. (2002). Interaction of nocodazole with tubulin isotypes. Drug Dev. Res. *55*, 91–96.